On the molecular diffusion coefficients of dissolved CO_2, HCO_3^-, and CO_3^{2-} and their dependence on isotopic mass

Richard E. Zeebe[*]

School of Ocean and Earth Science and Technology, University of Hawaii at Manoa, 1000 Pope Road, MSB 504, Honolulu, HI 96822, USA

Abstract

The molecular diffusion coefficients of dissolved carbon dioxide (CO_2), bicarbonate ion (HCO_3^-), and carbonate ion (CO_3^{2-}) are fundamental physico-chemical constants and are of practical significance in various disciplines including geochemistry, biology, and medicine. Yet, very little experimental data is available, for instance, on the bicarbonate and carbonate ion diffusion coefficient. Furthermore, it appears that no information was hitherto available on the mass-dependence of the diffusion coefficients of the ionic carbonate species in water. Here I use molecular dynamics simulations to study the diffusion of the dissolved carbonate species in water, including their dependence on temperature and isotopic mass. Based on the simulations, I provide equations to calculate the diffusion coefficients of dissolved CO_2, HCO_3^-, and CO_3^{2-} over the temperature range from 0° to 100 °C. The results indicate a mass-dependence of CO_2 diffusion that is consistent with the observed $^{12}CO_2/^{13}CO_2$ diffusion ratio at 25 °C. No significant isotope fractionation appears to be associated with the diffusion of the naturally occurring isotopologues of HCO_3^- and CO_3^{2-} at 25 °C.
© 2011 Elsevier Ltd. All rights reserved.

1. INTRODUCTION

The molecular diffusion coefficients of the dissolved carbonate species (CO_2, HCO_3^-, and CO_3^{2-}) in aqueous solution are fundamental physico-chemical parameters. Knowledge of these parameters at various temperatures is of practical value, for instance, in geochemical, biological, and medical applications. A few examples include sediment diagenesis, mineral precipitation and dissolution, fossil fuel carbon sequestration, industrial engineering, carbon uptake and calcification in phytoplankton and zooplankton, studies of duodenal ulceration, O_2/CO_2 exchange in red blood cells, and metabolic models of cornea-contact-lens systems (e.g. Berner, 1980; Uchida et al., 1983; Livingston et al.,

1995; Wolf-Gladrow and Riebesell, 1997; Zeebe, 2007b; Kaufmann and Dreybrodt, 2007; Berne et al., 2009; Chhabra et al., 2009). While the molecular diffusion coefficient of carbon dioxide in water is relatively well known over a range of temperatures, less is known about the bicarbonate diffusion coefficient, and little information is available on the diffusion coefficient of the carbonate ion.

As discussed below, diffusion coefficients of HCO_3^- and CO_3^{2-} at infinite dilution have been estimated based on conductivity measurements from the 1930s and 1940s (Robinson and Stokes, 1959; Li and Gregory, 1974). However, to the best of my knowledge, so far only a single experimental study has been conducted to directly determine the CO_3^{2-} diffusion coefficient in water. The few data points were published in a largely unknown short communication by a Japanese group in the 1960s (Kigoshi and Hashitani, 1963). Furthermore, it appears that diffusion studies of the ionic carbonate species have as yet been limited to temperatures ⩽ 30 °C. While some information is available on the mass-dependence of CO_2 diffusion in

---

[*] Address: School of Ocean and Earth Science and Technology, Department of Oceanography, University of Hawaii at Manoa, 1000 Pope Road, MSB 504, Honolulu, HI 96822, USA. Tel.: +1 808 956 6473; fax: +1 808 956 7112.
    E-mail address: zeebe@soest.hawaii.edu

water, e.g. on $^{12}CO_2$ vs. $^{13}CO_2$ diffusion (O'Leary, 1984; Jähne et al., 1987), I am not aware of a theoretical or experimental study that has hitherto tackled the mass-dependence of the diffusion coefficients of the bicarbonate and carbonate ion. The mass-dependence associated with the diffusion of the ionic carbonate species has implications, for instance, for understanding vital effects in carbonates and clumped isotope studies (e.g. Thiagarajan et al., 2009).

Given the geochemical, biological, and medical significance of the molecular diffusion coefficients of dissolved CO_2, HCO_3^-, and CO_3^{2-}, a comprehensive study of these important parameters appears warranted. From a geochemical point of view, such an effort also appears timely, given the growing number of studies dealing with the chemistry of dissolved CO_2 in seawater and the coupling of diffusion and reaction within the system (for fundamentals, see e.g. Wolf-Gladrow and Riebesell, 1997; Zeebe et al., 1999; Zeebe and Wolf-Gladrow, 2001). In the present study, I have used molecular dynamics (MD) simulations to examine the diffusion coefficients of the dissolved carbonate species in water, their temperature-dependence, and their dependence on isotopic mass. Among other results, I will provide equations to calculate the diffusion coefficients of the dissolved carbonate species over the temperature range from 0° to 100 °C.

Progress has recently been made in understanding diffusion processes using experimental as well as theoretical methods. This includes, for instance, laboratory experiments and molecular dynamics studies to elucidate the fundamentals of diffusion and the nature of ionic diffusion in aqueous solution and the influence of isotopic mass (Koneshan et al., 2001; Richter et al., 2006; Bourg and Sposito, 2007; Li et al., 2010). Several of these studies highlight the critical role of hydration for diffusion in liquid water, which is also fundamental to understanding hydrogen-bonding environments, solvation motifs, calcite growth, and carbon and oxygen isotope fractionation between dissolved compounds and water in thermodynamic equilibrium (e.g. Zeebe, 1999; Zeebe, 2007a; Rustad et al., 2008; Zeebe, 2009; Kumar et al., 2009; Garand et al., 2010; Raiteri et al., 2010; Zeebe, 2010).

Advances in computational power and numerical methods including molecular dynamics now allow accurate calculation of diffusion coefficients in many systems (see e.g. Section 5; Bourg and Sposito, 2007; Bourg and Sposito, 2008; Kerisit and Liu, 2010). The system of dissolved CO_2 in water is the focus of the present work. The manuscript is organized as follows. A few basics on diffusion and earlier estimates of ionic diffusion coefficients will be reviewed in Section 2. The methods employed in the present study and system-size effects on calculated diffusion coefficients will be described in Sections 3 and 4. Several tests allowing evaluation of the accuracy of MD-calculated diffusion coefficients will be provided in Section 5, while results for the carbonate species' diffusion coefficients and their mass-dependence will be presented and discussed in Sections 6 and 7. The errors involved in the present molecular dynamics simulations will be examined in Section 8. Finally, the conclusions will be given in Section 9.

2. SELF- AND TRACER-DIFFUSION COEFFICIENT

'Self-diffusion' is a process in which the molecules of, for instance, a uniform liquid move randomly over time from one point to another (Robinson and Stokes, 1959). 'Tracer-diffusion' usually refers to a process in which ions of a certain kind and of very small concentration diffuse in a large excess of other electrolyte. If both the tracer and the electrolyte are of the same nature, e.g. $^{22}Na^+$ in a sodium chloride solution, the tracer-diffusion coefficient is assumed to be equal to the self-diffusion coefficient.

2.1. Limiting conductivity

Limiting tracer- or self-diffusion coefficients of ions have been estimated based on measurements of the limiting conductivity using the Nernst–Einstein equation (Robinson and Stokes, 1959; Li and Gregory, 1974):

$$D^0 = \frac{R\,T\lambda^0}{z^2 F^2} \tag{1}$$

where D^0 is the limiting tracer- or self-diffusion coefficient, $R = 8.3145$ J K^{-1} mol^{-1} is the gas constant, T is temperature in Kelvin, λ^0 is the limiting conductivity (per mole), z is charge, and $F = 9.6485 \times 10^4$ C mol^{-1} is the Faraday constant. Using $\lambda^0_{HCO_3^-}$ and $\lambda^0_{CO_3^{2-}}$ of 4.45 and 13.86 m^2 mS mol^{-1} (Robinson and Stokes, 1959; Li and Gregory, 1974), the self-diffusion coefficients of HCO_3^- and CO_3^{2-} at 25 °C and infinite dilution may be estimated as 1.19 and 0.92×10^{-9} m^2 s^{-1}, respectively.

Considering ion mobility, a relation between conductivity and diffusion is to be expected. However, several fundamental differences exist. For instance, in conduction positive and negative ions move in opposite directions, whereas in diffusion they move in the same direction. Also, in conduction ions move independently at very low concentration, whereas in diffusion they have to move at equal speeds to ensure electroneutrality of the solution. Uncertainties in estimating self-diffusion coefficients based on conductivity data may arise from various issues, including the fact that conductivity measurements at finite concentration have to be extrapolated to zero concentration (for a detailed discussion of uncertainties, see Robinson and Stokes, 1959). Nevertheless, for a number of ions, measurement of the limiting conductivity (λ^0) provide quite accurate numbers for the self-diffusion coefficients.

In the case of HCO_3^- and CO_3^{2-}, the λ^0 values used in the past to estimate their diffusion coefficients (e.g. Li and Gregory, 1974) actually originate from conductivity measurements in the 1930s and 1940s (Shedlovsky and MacInnes, 1935; Monk, 1949). The conductivity measurements to derive $\lambda^0_{CO_3^{2-}}$ (Monk, 1949) showed drifts over time and required several corrections, including conductivity corrections for NaOH and NaHCO$_3$. Three different values of $\lambda^0_{CO_3^{2-}}$ at 25 °C are listed in Landolt-Börnstein (1960). Experimental values for $\lambda^0_{CO_3^{2-}}$ are available at 0°, 18°, and 25 °C, while measurement of $\lambda^0_{HCO_3^-}$ appears to be limited to 25 °C (Landolt-Börnstein, 1960). These data provide the basis for the values of the HCO_3^- and CO_3^{2-} diffusion coefficients frequently used in the literature. A comprehensive study of

these geochemically and biologically important parameters thus appears timely. It turns out that the conductivity-derived diffusion coefficients based on measurements from over 60 years ago are broadly consistent with the very limited data on the diffusion of the ionic carbonate species that are based on direct diffusion measurements. However, the values for $D_{CO_3^{2-}}$ at 25 °C, for example, which have been widely used in the literature and cited in textbooks (e.g. Boudreau, 1997; Reddi and Inyang, 2000; Hudak, 2005) are probably too high by 15–20%.

2.2. Stokes–Einstein temperature-dependence

The temperature-dependence of diffusion coefficients is often approximated using the Stokes–Einstein relation, which actually applies to spherical suspended particles (Einstein, 1905):

$$D = \frac{k_B T}{6\pi\eta R},\qquad(2)$$

where $k_B = 1.38 \times 10^{-23}$ kg m^2 s^{-2} K^{-1} is Boltzmann's constant, T is temperature, η is the shear viscosity, and R the radius of the particle. If D is known at temperature T_1, then $D(T)$ can be calculated from:

$$\frac{D(T)}{D(T_1)} = \frac{\eta(T_1)}{\eta(T)}\frac{T}{T_1}.\qquad(3)$$

The temperature-dependence of, for instance, diffusion coefficients of spherical suspended particles, can then be determined solely based on the shear viscosity of water (Huber et al., 2009). It is emphasized that the Stokes–Einstein relation does not apply to, for instance, ionic solutes in aqueous solution, supercritical water etc. (e.g. Kalinichev, 1993). Nevertheless, the temperature-dependence implied by Eq. (3) – not the Stokes–Einstein relation itself – also seems to hold approximately for the major seawater ions (Li and Gregory, 1974). The temperature-dependence of diffusion coefficients based on the Stokes–Einstein relation and based on molecular dynamics simulations for the dissolved ionic carbonate species will be compared in Section 6. The comparison is included here simply because the Stokes–Einstein relation has been widely used in the literature to estimate the temperature-dependence of various diffusion coefficients. It does not represent an alternative theory applicable to ions in liquid water.

3. METHODS

Diffusion coefficients were calculated based on molecular dynamics simulations using the portable program Moldy (version 3.6) (Refson, 2000), freely available at http://ccpforge.cse.rl.ac.uk/gf/project/moldy/frs. The program has been used to study various diffusion processes, including diffusion characteristics at clay–fluid interfaces, ionic mobilities in supercritical water, and the mass-dependence of ionic diffusion in liquid water (e.g. Leote de Carvalho and Skipper, 2001; Hyun et al., 2001; Bourg and Sposito, 2007). For the simulation of dissolved CO_2, HCO_3^-, and CO_3^{2-}, the unit simulation cell contained 215 water molecules plus one solute molecule or ion, unless stated

otherwise (Fig. 1). The $H_2O + CO_3^{2-}$ unit cell, for instance, was cubic with cell vector length 18.69 Å at a temperature of 298 K and density 1.0 g cm^{-3}. The program imposes periodic boundary conditions and treats molecules in the rigid approximation by solving the Newton–Euler equations of rotational dynamics. Simulations were initiated using the skew start method (Refson, 2000). Long-range Coulomb interactions were handled using the 3D Ewald sum technique with a typical cut-off distance of ∼9 Å. Pair-potentials were modeled using the Lennard–Jones potential:

$$U_{ij}(r) = 4\varepsilon_{ij}\left[\left(\frac{\sigma_{ij}}{r}\right)^{12} - \left(\frac{\sigma_{ij}}{r}\right)^{6}\right]\qquad(4)$$

where ε_{ij} and σ_{ij} are the Lennard–Jones parameters for atom pairs i and j. The minimum of the potential well is at $r = 2^{1/6}\sigma_{ij}$ and the value of the potential at this distance is $-\varepsilon_{ij}$. Note that σ_{ij} is effectively a size parameter (e.g. in het Panhuis et al., 1998). For the values of ε_{ij} and σ_{ij} used here, see below and Table 1.

Diffusion coefficients were calculated in two different ways during production runs after equilibration (see below). (i) From a fit to the mean square displacement, MSD(t), over the time interval in which MSD(t) increases linearly with time (Einstein, 1905):

$$6\,D\,t = \langle|\mathbf{r}(t) - \mathbf{r}(0)|^2\rangle = \text{MSD}(t),\qquad(5)$$

where $\mathbf{r}(t) = [x(t), y(t), z(t)]$ is the position of the particle at time t. (ii) From the velocity autocorrelation function, VAF(t) (Hansen and McDonald, 2006):

$$D = \frac{1}{3}\int_0^{t_u}\langle|\mathbf{v}(t)\cdot\mathbf{v}(0)|\rangle dt = \frac{1}{3}\int_0^{t_u}\text{VAF}(t)dt\qquad(6)$$

where $\mathbf{v}(t) = [u(t), v(t), w(t)]$ is the particle velocity and t_u is the upper time integration limit (note: while $t_u \rightarrow \infty$
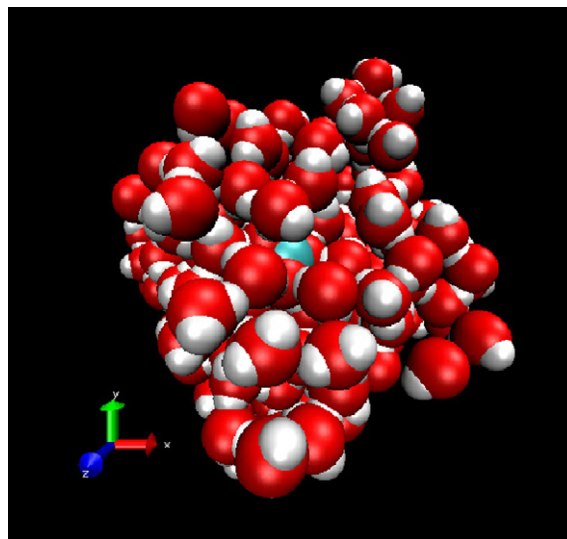

Fig. 1. Molecular dynamics (MD) simulation cell used in standard simulations: 215 water molecules plus one solute molecule or ion. Example shows the carbonate ion (CO_3^{2-}), blue = carbon, red = oxygen, white = hydrogen. Visualization: VMD (Humphrey et al., 1996).

Table 1
MD simulation parameters for Lennard–Jones potentials and partial charges.

Pair $i-j$	ε_{ij} (kJ mol^{-1})	σ_{ij} (Å)	[a]q_j	Ref.
$O_{H_2O} - O_{H_2O}$	0.65015	3.1656	−0.8476	[b]
$O_{H_2O} - C_{CO_2}$	0.51369	3.2618	+0.6172	[c]
$O_{H_2O} - O_{CO_2}$	0.81057	3.0145	−0.3086	[c]
$O_{H_2O} - C_{HCO_3^-}$	0.24112	2.7850	+1.1230	[d]
$O_{H_2O} - O(1)_{HCO_3^-}$[e]	0.65015	3.1656	−0.7907	[f]
$O_{H_2O} - O(2)_{HCO_3^-}$[e]	0.65015	3.1656	−0.8985	[f]
$O_{H_2O} - O(3)_{HCO_3^-}$[e]	0.65015	3.1656	−0.8338	[f]
$O_{H_2O} - H_{HCO_3^-}$	–	–	+0.4000	[f]
$O_{H_2O} - C_{CO_3^{2-}}$	0.24112	2.7850	+1.1230	[d]
$O_{H_2O} - O_{CO_3^{2-}}$	0.65015	3.1656	−1.0410	[d]

[a] Partial charge on atom j.
[b] Berendsen et al. (1987).
[c] in het Panhuis et al. (1998).
[d] Wang and Becker (2009).
[e] Label 1 denotes O of the O−H group, 2 and 3 the remaining O proximal and distal to H, respectively.
[f] Wang and Becker (2009), Duffy et al. (2005). Partial charges from *ab initio* calculations (see text).

theoretically, in practice t_u may be rather small). The two methods and the associated errors are discussed in detail in Section 8.

For the calculation of the diffusion coefficients of dissolved CO_2, HCO_3^-, and CO_3^{2-}, sets of sixteen production runs over 500 ps were performed (see below) with constant numbers of particles, volume, and energy for each run (microcanonical or NVE ensemble). Maximum changes in total energy over the 500 ps time span were typically less than 0.1%. The temperature – pressure – volume (TVP) relationship for the run was set by the input parameters temperature and density. The density was adjusted at different temperatures to maintain approximately constant pressure using a temperature–density relationship for the water model used here (see Section 5.2).

3.1. CPU-ensemble approach

The numerical computation of diffusion coefficients requires averaging over long time intervals and/or large ensemble sizes for statistical reasons (see Section 8). For example, for the diffusion of a single ion in aqueous solution (ensemble size $n_e = 1$), simulation times are typically of order ns, which requires $\sim 10^6$ numerical steps at a time step of $\Delta t = 0.001$ ps. In the present study, I used a 16-CPU cluster to run sixteen simultaneous 500 ps-long simulations with different initial conditions for a given solute ('CPU-ensemble', $n_e = 16$). Runs were preceded by temperature equilibration of 2 ps at $\Delta t = 0.0001$ ps and 100 ps at $\Delta t = 0.001$ ps (Bourg and Sposito, 2007). Note that each instance of the program was run on one processor in sequential mode using the serial version of the code (not the parallel version). The 16 simulations were set up with different 'initial conditions' by performing short scaling runs before equilibration with different numbers of steps between scalings for each run. This led to rapid divergence

of trajectories and velocities between runs, as confirmed by the variability in the mean square displacement (MSD) and the velocity autocorrelation function (VAF) of the CPU-ensemble (see inlet Figs. 2a and 3).

In addition, possible correlations between runs were checked by calculating correlation coefficients $R_{ij}^r = \text{corr}(|\mathbf{r}_i(t)|, |\mathbf{r}_j(t)|)$ and $R_{ij}^v = \text{corr}(|\mathbf{v}_i(t)|, |\mathbf{v}_j(t)|)$, where $\mathbf{r}_i(t)$ and $\mathbf{v}_i(t)$ refer to solute coordinates and velocities, and $i, j = 1, \ldots, 16 (i \neq j)$. These may be compared to correlations within a single run, for instance, between the first and second half of a given run $R_{i,t}^r = \text{corr}(|\mathbf{r}_i(t')|, |\mathbf{r}_j(t'')|)$, where $\{0 \leqslant t' \leqslant t_r/2\}, \{t_r/2 < t'' \leqslant t_r\}$, and t_r is total run time. For example, for CO_3^{2-} at 298 K, the absolute means of the correlation coefficients are $\overline{R_{ij}^r} \simeq 0.3$ and $\overline{R_{ij}^v} \simeq 0.0004$, while $\overline{R_{i,t}^r} \simeq 0.1$ and $\overline{R_{i,t}^v} \simeq 0.002$. These numbers indicate little difference in the correlation of variables between multiple runs with different initial conditions on the one hand (CPU-ensemble), and the correlation of variables within a single run on the other (time series). This is corroborated by the variability in MSD and VAF (see
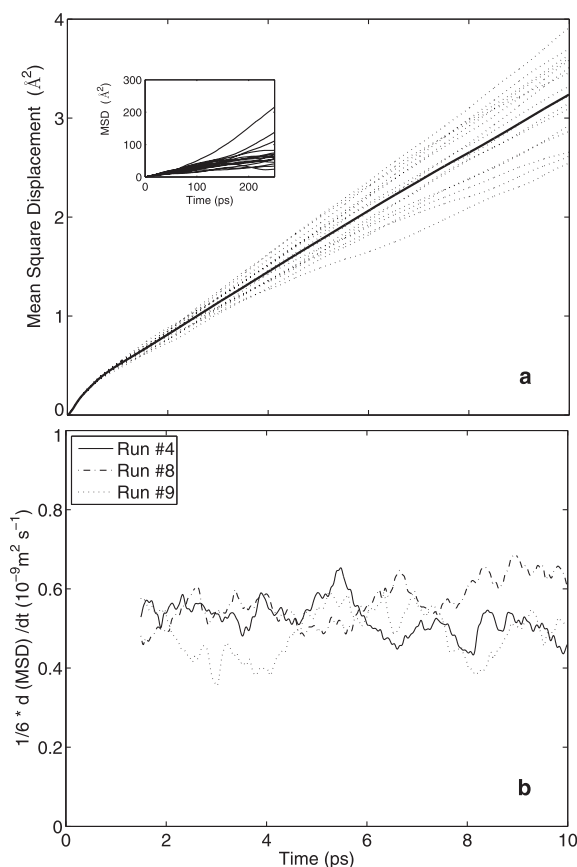

Fig. 2. (a) Example of MD-calculated mean square displacement of CO_3^{2-} at 298 K based on a set of 16 simulations (dotted lines). The solid line indicates the mean value of all runs. Note that results shown are for $N = 216$ (to obtain final values, system-size correction needs to be applied). Inlet: note different axes limits. (b) The quantity $1/6 \times \text{d(MSD)}/\text{d}t$ used for time series error analysis (see text) shown for three arbitrary runs from the set of 16.
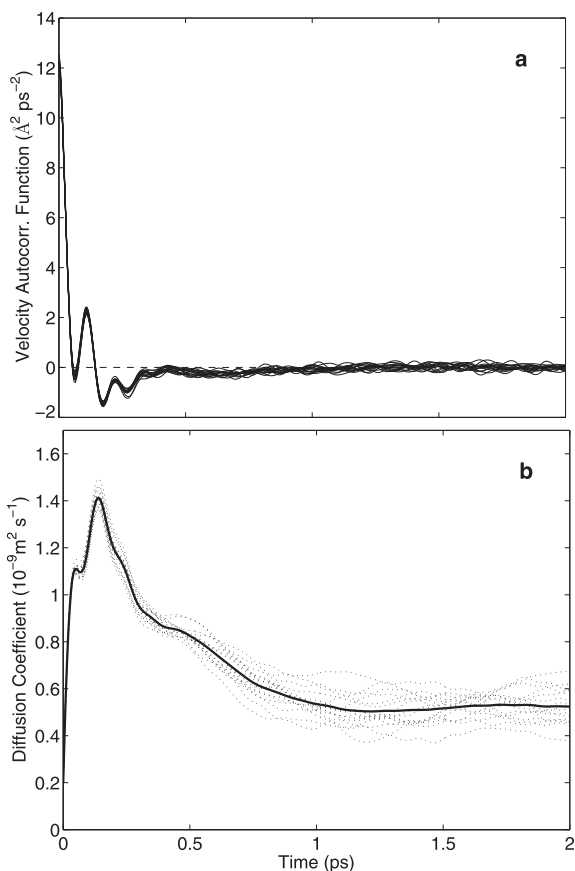
Fig. 3. (a) Example of MD-calculated velocity autocorrelation function $VAF(t)$ of CO_3^{2-} at 298 K based on a set of 16 simulations. (b) Diffusion coefficient calculated by integrating $VAF(t)$ over time (see text). Dotted lines: all 16 runs; solid line: mean value.

Section 8) and is to be expected if the system is ergodic (ensemble averages and time averages are equivalent).

On a parallel cluster, the CPU-ensemble used here for the simulation of solute diffusion is computationally cost-effective. For a 16-CPU cluster, the method effectively provides the equivalent of a serial 16-ns run for the time cost of a 1-ns run. Also, using multiple CPUs for multiple sequential runs allows simultaneous computation of MSD and VAF (which can be time-consuming), once the MD simulations have been completed.

3.2. Water model

For the MD simulations of the present study, the extended simple point charge (SPC/E) model for water was used (Berendsen et al., 1987). The rigid SPC/E water model has a fixed O–H bond length of 1 Å and an HOH angle of 109.47°. The point charges and Lennard–Jones parameters are summarized in Table 1. Note that the MD-calculated self-diffusion coefficient of water depends on the size of the simulation cell (e.g. Dünweg and Kremer, 1991; Dünweg and Kremer, 1993; Yeh and Hummer, 2004; Kerisit and Liu, 2010). At a cubic cell length of ~ 19 Å ($N = 216$) and at 25 °C, the self-diffusion coefficient of the SPC/E water model agrees well with observations. However, this

is not the case at different cell lengths and all temperatures over the range 0–100 °C (see Sections 4 and 5.2).

3.3. Solute models

The Lennard–Jones parameters, partial charges and C–O bond length (1.162 Å) for dissolved CO_2 were taken from in het Panhuis et al. (1998), see Table 1. The Lennard–Jones parameters for oxygen and carbon for HCO_3^- and CO_3^{2-} and the partial charges for CO_3^{2-} were taken from Wang and Becker (2009), who used the parameters for the carbonate ion in the vaterite mineral ($CaCO_3$). Note, however, that the parameters were originally used in aqueous solution (Kalinichev et al., 2001). The O–H bond length in HCO_3^- was set to 0.96 Å, the C–O–H bond angle to 115°, and the hydrogen partial charge to $+0.4e$ (Duffy et al., 2005). To maintain charge balance, Duffy et al. (2005) raised the charge of the oxygen atom of the O–H group in HCO_3^- by $0.6e$ and left the charges of the remaining two oxygen unchanged (relative to the partial charges in CO_3^{2-}).

However, I performed *ab initio* calculations using GAMESS (Gordon and Schmidt, 2005), which indicated that the charge is distributed more homogeneously among the three oxygen atoms of the bicarbonate ion. After geometry optimization based on e.g. HF/6-31G(d) and B3-LYP/6-31++G(d), charge fitting to the electrostatic potential gave a charge ratio of $q_{O_1} : q_{O_2} : q_{O_3} \simeq 1 : 1.14 : 1.05$, where O_1 denotes the O of the O–H group, and O_2 and O_3 the remaining O proximal and distal to H, respectively. I tested two different levels of theory with and without diffuse functions and three different charge fit methods, which all gave very similar results. In addition, I calculated the HCO_3^- partial charges including a continuum solvent model for water. While the resulting charge distribution was slightly different, the effect on the HCO_3^- diffusion coefficient was insignificant (for instance, 1.14 ± 0.04 vs. 1.12 ± 0.04 based on MSD at 298 K). Consequently, the oxygen partial charges of HCO_3^- were set according to the charge ratio obtained from *ab initio* calculations. The parameters for the solute models are summarized in Table 1.

The calculated radial distribution functions ($g(r)$, Fig. 5) and hence the coordination numbers of the solute species agree very closely with those obtained from *ab initio* molecular dynamics methods (Leung et al., 2007; Rustad et al., 2008; Kumar et al., 2009). For CO_2, the similarity between radial distribution functions of classical force field studies (in het Panhuis et al., 1998) and *ab initio*-MD methods was noted previously (Leung et al., 2007). One minor difference appears to be the fact that the first peak in $g_{C-O_w}(r)$ of the present CO_3^{2-} model occurs at a slightly shorter distance compared to *ab initio*-MD results (Rustad et al., 2008; Kumar et al., 2009).

4. SYSTEM-SIZE DEPENDENCE OF DIFFUSION COEFFICIENTS

Long-range interactions in molecular dynamics simulations with finite system size and periodic boundary conditions can lead to significant effects on the simulated

diffusion coefficient (Dünweg and Kremer, 1991; Dünweg and Kremer, 1993; Yeh and Hummer, 2004; Kerisit and Liu, 2010). In agreement with these studies, the present simulations yielded a significant increase in D_{H_2O} ($\sim 25\%$ at 298 K) as the system size tended from $N = 128$ towards infinity, i.e. as the inverse of the simulation's cell box length (L) tended towards zero (Fig. 4). In fact, it can be shown theoretically that the simulated diffusion coefficient should depend inversely on L (Dünweg and Kremer, 1991; Yeh and Hummer, 2004). The diffusion coefficient at infinite system size D_i^∞ may be obtained from:

$$D_i^\infty = D_i^{MD} + \frac{\zeta k_B T}{6\pi\eta(T)L}, \qquad (7)$$

where D_i^{MD} is the MD-calculated diffusion coefficient of species i at the system size of the simulation, $\zeta = 2.837297$ arises from Ewald summation in a cubic lattice, and $\eta(T)$ is the simulated shear viscosity at temperature T. Note that Eq. (7) applies to both solute and solvent. The final calculated value should of course be independent of the size of the simulation cell. Thus the size-independent solute-to-solvent ratio of diffusion coefficients is determined first, from which the final diffusion coefficient of solute species i is calculated as:

$$D_i = D_i^\infty \frac{D_{H_2O}^{exp}}{D_{H_2O}^\infty}, \qquad (8)$$

where $D_{H_2O}^{exp}$ is the observed diffusion coefficient of water (e.g. Holz et al., 2000).

As mentioned above, Eq. (7) applies to both solute and solvent. Indeed, the slopes of $D_{H_2O}^{MD}$ and $D_{CO_3^{2-}}^{MD}$ as a function of $1/L$ as derived here at 298 K are essentially the same (Fig. 4). This is critical for the calculated solute-to-solvent ratio of diffusion coefficients, particularly for species with significantly smaller or larger diffusion coefficients than water. For instance, at 298 K and $N = 216$, the VAF-calculated $D_{CO_3^{2-}}^{MD}$ equals 0.53×10^{-9} m^2 s^{-1} and $D_{CO_3^{2-}}^{MD}/D_{H_2O}^{MD} =$

Fig. 5. Calculated radial distribution functions of the dissolved carbonate species at 298 K. C = central carbon atom in (a) CO_2, (b) HCO_3^-, and (c) CO_3^{2-}; O_w/H_w = oxygen/hydrogen of water.

0.22. However, at infinite system size, $D_{CO_3^{2-}}^\infty = (0.53 + 0.48) \times 10^{-9}$ m^2 s^{-1} = 1.01×10^{-9} m^2 s^{-1} (see Eq. (7)) and $D_{CO_3^{2-}}^\infty/D_{H_2O}^\infty = 0.35$ (Fig. 4, Table 4). Using Eq. (8), the final VAF-calculated diffusion coefficient of the carbonate ion at 298 K is $D_{CO_3^{2-}} = 1.01 \times 10^{-9} \times 2.29/2.85$ m^2 s^{-1} = 0.81×10^{-9} m^2 s^{-1} (Table 4).

5. TESTING DIFFUSION COEFFICIENTS CALCULATED FROM MOLECULAR DYNAMICS SIMULATIONS

Before using molecular dynamics simulations to tackle diffusion properties that have not been studied until present, it is instructive to test whether the methods employed here produce results that are in agreement with independent theoretical and observational results. This includes, for instance, values of diffusion coefficients of solvent and solute, their temperature-dependence, and the mass-dependence of different isotopologues. In the following, molecular dynamics will be applied to noble gas diffusion and their mass-dependence and the temperature-dependence of the self-diffusion coefficients of water and dissolved CO_2. Examinations of MD-simulated diffusion and mobility of dissolved ions and noble gases, and their mass-dependence
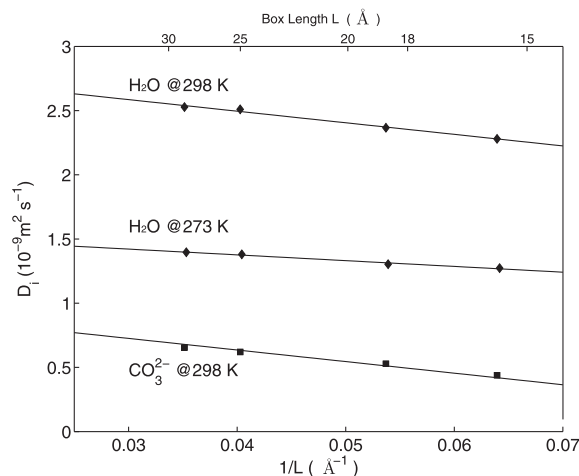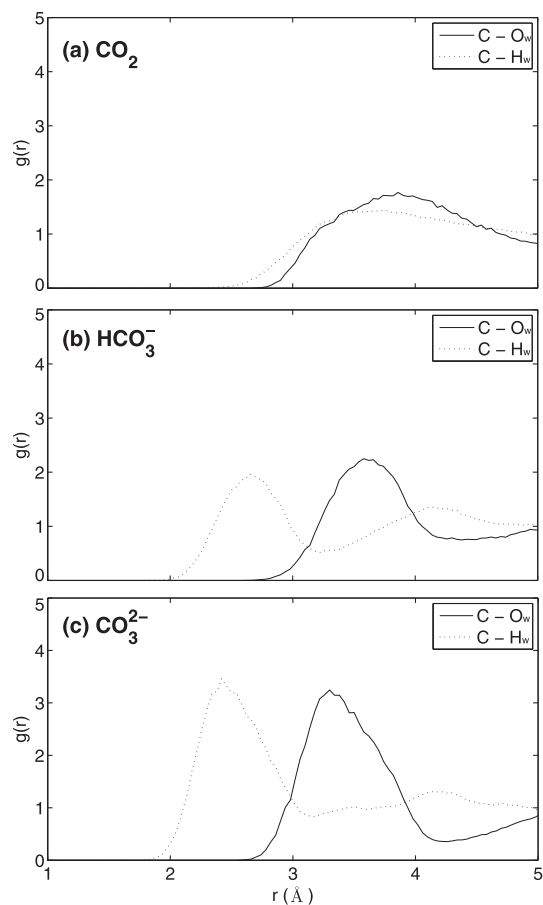
Fig. 4. System-size dependence of MD-calculated diffusion coefficients. Diffusion coefficients of solute and solvent increase linearly as $1/L \to 0$ (i.e. $L \to \infty$, where L is the box length of the cubic unit cell).

have been reported earlier (e.g. Koneshan et al., 2001; Bourg and Sposito, 2007; Bourg and Sposito, 2008; Kerisit and Liu, 2010).

5.1. Noble gases and mass-dependence

The following section is relevant to the calculation of the mass-dependence of the carbonate species (Section 6.2). Before using MD simulations to predict the yet unknown mass-dependence of the ionic carbonate species for which no observational or theoretical comparison exists so far, it is useful to test whether or not the MD simulations reproduce the known mass-dependence of a monoatomic noble gas.

Based on first principles, the Chapman–Enskog theory predicts the self-diffusion coefficient of a gas consisting of spherically symmetrical molecules as (Chapman and Cowling, 1970):

$$D_g^s = \frac{3}{8} \frac{k_B\, T}{P\, d^2\, W} \left(\frac{k_B\, T}{\pi\, m} \right)^{1/2}, \tag{9}$$

where $k_B = 1.38 \times 10^{-23}$ kg m^2 s^{-2} K^{-1} is Boltzmann's constant, T is temperature, P is pressure, d is the collision diameter, and m is the mass. The collision integral W depends on the type of interaction between the molecules (see Chapman and Cowling, 1970). Eq. (9) shows that D_g^s should be $\propto T^{3/2}$, inversely proportional to P, and proportional to $m^{-1/2}$. The Chapman–Enskog predictions agree well with observations. For instance, using $m = 39.95$ amu, $d = 3.54$ Å, and $W = 0.935$ (Cussler, 1984), the predicted self-diffusion coefficient of argon is $D_{Ar} = 0.182 \times 10^{-4}$ m^2 s^{-1} at 295 K and 1 atm. The corresponding observed value is 0.178×10^{-4} m^2 s^{-1} (Winn, 1950). For Ne at 300 K and 1 atm, the predicted and observed values are 0.517×10^{-4} m^2 s^{-1} and 0.516×10^{-4} m^2 s^{-1} (Winn, 1950), respectively.

The D_g^s's of noble gases predicted by Eq. (9) at 300 K and 1 atm and those summarized in Kestin et al. (1984) are shown in Fig. 6. Also shown are results of the present

Fig. 6. Diffusion coefficients of noble gases. Calculations using Chapman–Enskog theory are based on Eq. (9). The simulated mass-dependence of D_{Ar} is in agreement with the theoretical slope of $-1/2$ for spherically symmetrical molecules (dotted lines).

study for variable Ar mass based on MD simulations with Lennard–Jones parameters $\varepsilon_{ij} = 0.9977$ kJ mol^{-1} and $\sigma_{ij} = 3.4$ Å (e.g. Rahman, 1964; Allen and Tildesley, 1987). Note that for statistical reasons, the simulations were performed at $T = 140$ K, $\rho = 0.035$ g cm^{-3} ($P = 9.3$ atm). Under these conditions (as well as at room temperature) Ar is a gas experimentally (Tegeler et al., 1999) and in the simulations. Yet the simulations are significantly less time consuming than, for instance, at 300 K and 1 atm. The MD-based diffusion coefficients have been plotted so that the calculated D_{Ar} (at mass 39.95 amu) matches the observed D_{Ar} at 300 K and 1 atm for comparison with the D_g^s's of noble gases (Fig. 6). Several conclusions can be drawn. First, the collision parameters σ and W of the noble gas series (He, Ne, Ar, Kr, Xe) cause a stronger decrease of the self-diffusion coefficient than expected from the mass-dependence alone (slope $< -1/2$ in a log–log plot, Fig. 6). Second, the features of noble gas diffusion are well captured by the Chapman–Enskog theory, including the well-known m$^{-1/2}$-dependence of the diffusion coefficient of a monoatomic noble gas (Eq. (9)). As mentioned above, this refers to a gas consisting of spherically symmetrical molecules, not to gas mixtures or fluids. Finally, the numerical results for variable Ar mass (diamonds) show that the results of the present MD simulations are in agreement with the theoretically predicted mass-dependence of slope $= -1/2$ for spherically symmetrical molecules (dotted lines). While this is no guarantee that the MD simulations correctly predict the diffusion mass-dependence in aqueous systems, it confirms that the MD simulations correctly predict the diffusion mass-dependence in simple gas systems.

5.2. Water self-diffusion coefficient vs. temperature

One critical prerequisite for appropriate simulation of solute diffusion is an adequate self-diffusion coefficient of the solvent itself. As mentioned above, the SPC/E water model was used in the present study (Berendsen et al., 1987). Observations of the self-diffusion coefficient of water (D_{H_2O}) are numerous and can be represented over the temperature range 0–100 °C with an error limit of $\leqslant 1\%$ by (Holz et al., 2000):

$$D_{H_2O} = D_{H_2O}^0 \left[(T/T_S) - 1 \right]^\gamma \tag{10}$$

where $D_{H_2O}^0 = 16.35 \times 10^{-9}$ m^2 s^{-1}, $T_S = 215.05$ K, and $\gamma = 2.063$. The self-diffusion coefficient of the SPC/E water model agrees well with observations at a cubic cell length of ~ 19 Å ($N = 216$) and at 25 °C (Fig. 7). However, this is not the case at different cell lengths and different temperatures. At $N = 216$, the calculated temperature-dependence is too weak and the simulations significantly underestimate D_{H_2O} above 50 °C (Fig. 7). While the calculated, size-independent water diffusion coefficient ($N \to \infty$) shows an improved temperature-dependence, it overestimates D_{H_2O} over the entire temperature range from 0° to 100 °C (Fig. 7). Caution is therefore advised when using absolute values of the water diffusion coefficient based on the SPC/E model at varying system size or temperature. For solute diffusion, these issues can be addressed by using Eq. (8),
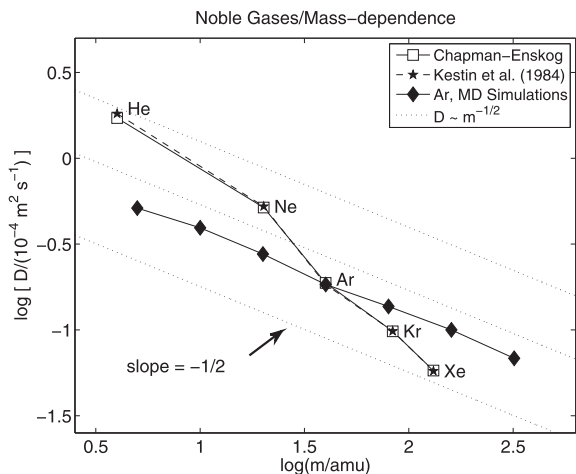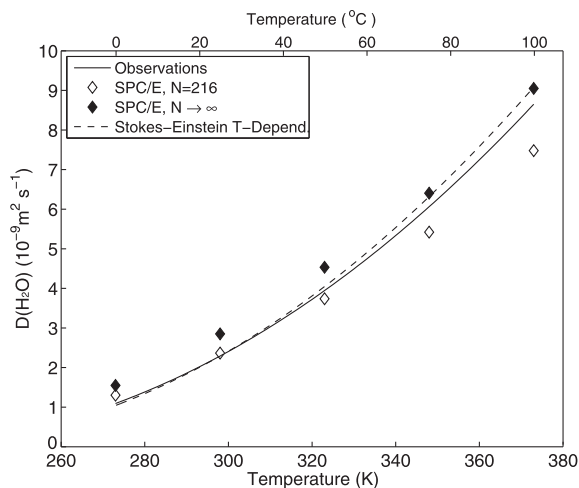
Fig. 7. Water diffusion coefficient based on observations (solid line, Holz et al., 2000) and present MD simulations at $N = 216$ (open diamonds) and $N \rightarrow \infty$ (closed diamonds), see text. Dashed line: T-dependence based on Stokes–Einstein relation relative to observed value at 25 °C.

Fig. 8. Diffusion coefficient of dissolved CO_2 based on observations and present MD simulations (diamonds). Confidence intervals (95%) of simulated values are based on ensemble statistics. Solid line: fit to simulated values (see text). Dashed line: T-dependence based on Stokes–Einstein relation relative to calculated value at 25 °C.

which corrects for system-size effects and normalizes to the observed D_{H_2O}.

Furthermore, the simulated diffusion coefficient of water depends on the pressure of the simulation cell. In order to adjust the input density parameter to maintain approximately constant pressure during production runs at different temperatures ($V = $ const. during individual runs), a temperature-density relationship for the SPC/E water model was obtained based on a separate set of runs at constant pressure. Over the temperature range from 273 to 373 K, the T-ρ-relationship for the water model and the present simulation cell ($N = 216$) may be represented as:

$$\rho_{SPC/E} = 6.8869 \times 10^{-1} + 3.5308 \times 10^{-3} \times T$$
$$- 1.1268 \times 10^{-5} \times T^2 + 9.7349 \times 10^{-9} \times T^3 \quad (11)$$

where T is in Kelvin. At a given input temperature, Eq. (11) was used to determine the input density for the simulations. Note that small variations in density/pressure have a minor effect on the calculated diffusion coefficients. For example, at 348 K and $\rho = 0.9631$ vs. $\rho = 0.9550$ (~ 15 MPa pressure difference), the calculated D_{CO_2}'s are identical within errors. On the contrary, factors such as the system size have a much larger effect. For example, D_{CO_2} increases by 21% at 348 K as N tends from 216 towards infinity (Table 4).

5.3. Dissolved CO_2

Using the SPC/E water model, MD parameters for dissolved CO_2 given by in het Panhuis et al. (1998), and Eq. (8), the computed CO_2 diffusion coefficient at 298 K based on VAF equals $2.02 \pm 0.19 \times 10^{-9}$ m^2 s^{-1} (Table 4). This is in good agreement with observations (Fig. 8). Note that the confidence interval given here reflects the statistics of the simulations, rather than biases due to systematic errors (for detailed discussion, see Section 8). The simulated values agree well with observations over the temperature range
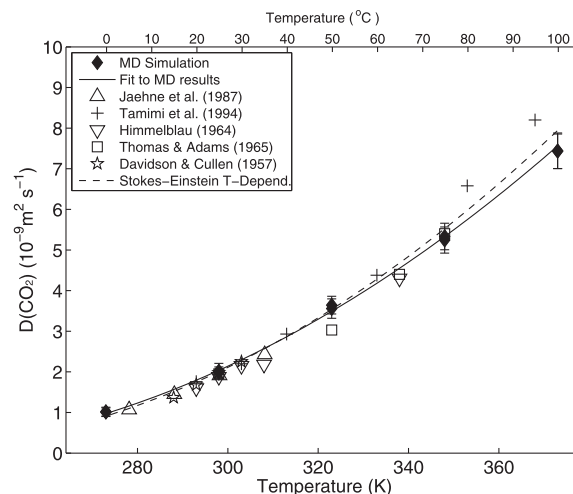
0–75 °C (Davidson and Cullen, 1957; Himmelblau, 1964; Thomas and Adams, 1965; Jähne et al., 1987; Tamimi et al., 1994). The two data points above 75 °C (Tamimi et al., 1994) indicate higher values than the simulations. However, note that Tamimi et al.'s values are also higher than other observational results across the entire temperature range.

6. RESULTS

The tests described in the previous section indicate that reliable diffusion coefficients can be obtained from molecular dynamics simulations, if carefully applied (taking into account system-size effects, for instance). In the following, MD-based results for the diffusion coefficients of HCO_3^- and CO_3^{2-} and their mass-dependence will be presented, for which little or no experimental data is currently available.

6.1. Diffusion coefficients of dissolved CO_2, HCO_3^-, and CO_3^{2-}

The MD-calculated diffusion coefficients of dissolved CO_2, HCO_3^-, and CO_3^{2-} as a function of temperature are shown in Figs. 8–10 (for discussion including experimental results, see Section 7). Over the temperature range 0–100 °C, a power-law equation (Speedy and Angell, 1976) was fit to the MD-calculated diffusion coefficients for CO_2, HCO_3^-, and CO_3^{2-}:

$$D_i = D_i^0 \left[(T/T_i) - 1 \right]^{\gamma_i} \quad (12)$$

where D_i^0, T_i, and γ_i are fit parameters for the individual carbonate species i (Table 2). Note that the choice of the fit equation is somewhat arbitrary, given the uncertainties of the calculations. However, Eq. (12) resulted in a much
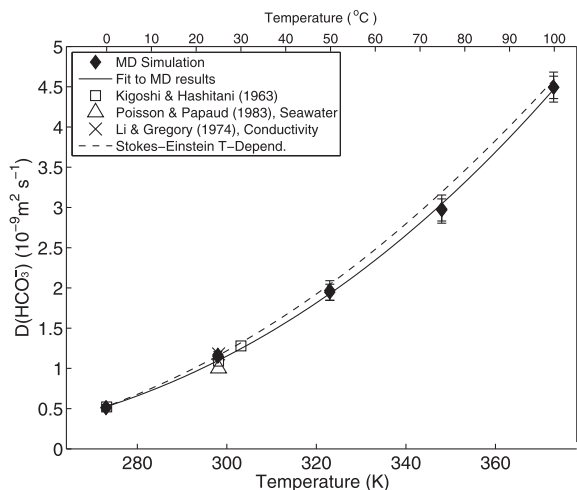
Fig. 9. Diffusion coefficient of dissolved HCO_3^- based on observations (squares, triangle) and present MD simulations (diamonds). Confidence intervals (95%) of simulated values are based on ensemble statistics. Solid line: fit to simulated values (see text). Cross: $D_{HCO_3^-}$ at 25 °C based on limiting conductivity. Dashed line: T-dependence based on Stokes–Einstein relation relative to calculated value at 25 °C.
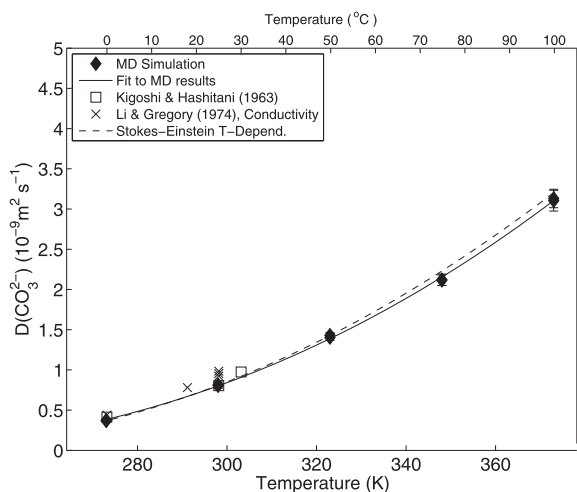

Fig. 10. Diffusion coefficient of dissolved CO_3^{2-} based on observations (squares) and present MD simulations (diamonds). Confidence intervals (95%) of simulated values are based on ensemble statistics. Solid line: fit to simulated values (see text). Crosses: $D_{CO_3^{2-}}$ based on limiting conductivity. Dashed line: T-dependence based on Stokes–Einstein relation relative to calculated value at 25 °C.

Table 2
Fit parameters for MD-calculated diffusion coefficients.[a]

Diffusion coefficient	Temp. range (K)	D_i^0 (10^{-9} m² s⁻¹)	T_i (K)	γ_i (−)
D_{CO_2}	273 – 373	14.6836	217.2056	1.9970
$D_{HCO_3^-}$	273 – 373	7.0158	204.0282	2.3942
$D_{CO_3^{2-}}$	273 – 373	5.4468	210.2646	2.1929

[a] Results were fitted to $D_i = D_i^0 \left[(T/T_i) - 1 \right]^{\gamma_i}$, where T is in K.
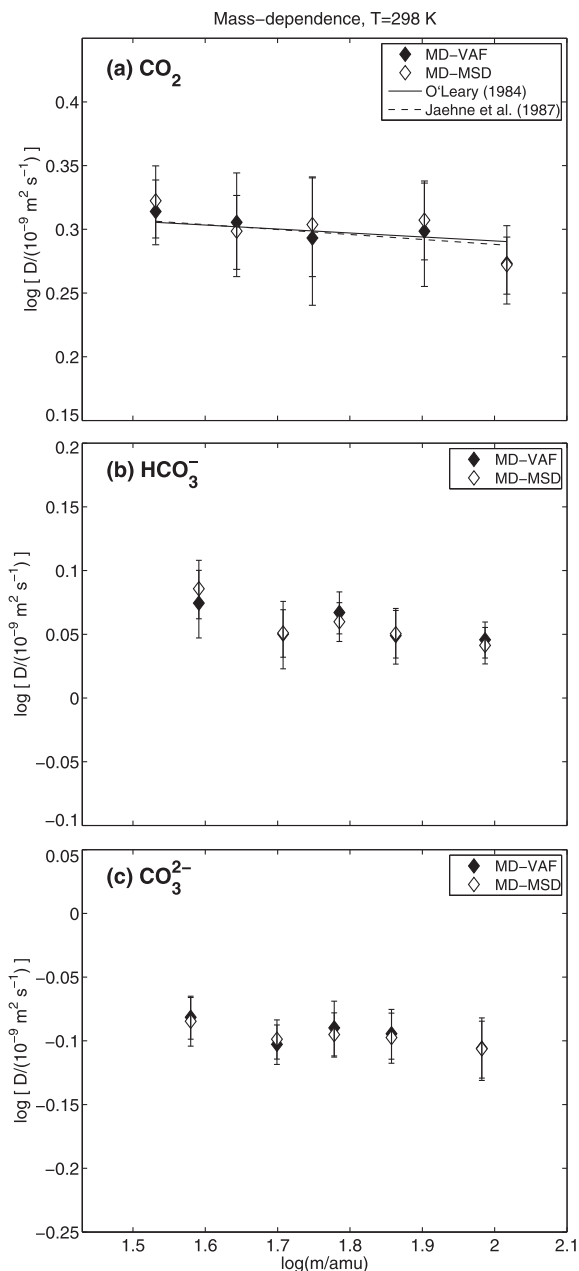

Fig. 11. Mass-dependence of diffusion coefficients at 298 K (m = molecular mass). (a) CO_2: closed diamonds indicate results of MD simulations based on velocity autocorrelation function (VAF). Open diamonds: based on mean square displacement (MSD). Confidence intervals (95%) of simulated values are based on ensemble statistics, see text. The solid and dashed lines indicate observed mass-dependence during $^{12}CO_2/^{13}CO_2$ diffusion. (b) HCO_3^- simulations. (c) CO_3^{2-} simulations.

better fit than, for instance, a fit based on an Arrhenius equation or a polynomial. This is not surprising because the temperature dependence of the solutes is mostly determined by the observed temperature-dependence of water (Eq. (8)), which follows the same power-law (Eq. (10)). Minor contributions come from variations in the ratio $r^\infty = D_i^\infty / D_{H_2O}^\infty$ (Table 4).

The dashed lines in Figs. 8–10 indicate the temperature-dependence according to the Stokes–Einstein relation (Eq. 3), relative to the calculated value at 25 °C. Note that the Stokes–Einstein temperature-dependence is included here simply because it has been widely used in the literature. It does not represent an alternative theory applicable to ions in liquid water.

6.2. Isotopic mass

To examine the dependence of CO_2 diffusion on isotopic mass, the carbon mass in CO_2 was varied between hypothetical values of 2 and 72 amu at 298 K. In other words, diffusion coefficients were calculated for $^{12}C^{16}O_2$ and the fictitious molecules $^2C^{16}O_2$, $^{24}C^{16}O_2$, $^{48}C^{16}O_2$, and $^{72}C^{16}O_2$ with molecular masses $m = 34, 44, 56, 80$, and 104 (Fig. 11a). Note that simulations spanning only the small mass-range of naturally occurring isotopes would not allow to deduce meaningful trends of calculated diffusion coefficients vs. isotopic mass. This is due to the statistical uncertainty in the mean value of calculated diffusion coefficients (see Section 8). For instance, the reported values for carbon isotope fractionation during $^{12}CO_2/^{13}CO_2$ diffusion are 0.7‰ (25 °C) and 0.87‰ (O'Leary, 1984, 1987). In contrast, the 95% confidence interval of the present MD simulations is several percent of the calculated mean value (Section 8, Fig. 11).

The results of the MD simulations at different CO_2 masses indicate a small isotope effect for CO_2 diffusion, consistent with observations (Fig. 11a). However, the statistical uncertainties of the simulations impede precise calculation of the isotopic fractionation. For the VAF-calculated diffusion coefficients, a simple linear regression (random Gaussian errors) of $\log(D_{CO_2}/\mathscr{D}_0)$ vs. $\log(m/m_0)$ yields slopes between -0.14 and -0.01 at the 95% confidence level ($\mathscr{D}_0 = 10^{-9}$ m^2 s^{-1}, $m_0 = 1$ amu). For comparison, the observed slopes are -0.03 and -0.04. The mass-dependence of HCO_3^- and CO_3^{2-} diffusion was examined based on simulations at 298 K using carbon masses 2, 12, 24, and 48 at oxygen mass 16 and carbon mass 2 at oxygen mass 12. The results are shown in Fig. 11b and c as a function of the molecular mass m on a logarithmic scale (horizontal axis). For HCO_3^-, the VAF-based slopes ranged from -0.17 to $+0.04$ at the 95% confidence level. For CO_3^{2-}, the corresponding slopes ranged from -0.13 to $+0.04$.

7. DISCUSSION

Sufficient experimental data is available on CO_2 diffusion in water to evaluate the MD simulations of dissolved CO_2. As mentioned above, while observations and simulations of D_{CO_2} show good agreement from 0 to 75 °C (Fig. 8), the two data points above 75 °C (Tamimi et al., 1994) indicate higher values than the simulations. However, Tamimi et al.'s numbers are also higher than other observational results across the entire temperature range. The MD-predicted temperature-dependence of D_{CO_2} is slightly less than the Stokes–Einstein temperature-dependence (Eq. 3).

Significantly less experimental data have been published on HCO_3^- diffusion (Fig. 9). A few measurements of $D_{HCO_3^-}$ in NaHCO$_3$ solutions were conducted at 0, 25, and 30 °C (Kigoshi and Hashitani, 1963; Hashitani and Kigoshi, 1965). Their value for $D_{HCO_3^-}$ at 25 °C appears to be slightly higher than the value obtained in seawater (Poisson and Papaud, 1983).

The estimates of diffusion coefficients based on limiting conductivity for both HCO_3^- and CO_3^{2-} (Li and Gregory, 1974) are higher than the experimental values (crosses in Figs. 9 and 10). This could be due to general limitations involved in deriving diffusion coefficients from conductivity data (see Section 2.1). Alternatively, the conductivity-based values could be higher because they actually apply to infinite dilution, whereas diffusion experiments are conducted at finite dilution. Overall, the MD-calculated results are in good agreement with the sparse direct observations, given uncertainties in force fields, etc. The direct diffusion measurements and the present MD simulations suggest that the values of 0.92 and 0.96 × 10^{-9} m^2 s^{-1} for $D_{CO_3^{2-}}$ at 25 °C (Robinson and Stokes, 1959; Li and Gregory, 1974) that have been widely used in the literature and cited in textbooks (e.g. Boudreau, 1997; Reddi and Inyang, 2000; Hudak, 2005) are probably too high by 15–20%.

It seems desirable to clarify these issues in a comprehensive experimental study that examines various effects including temperature, concentrations, ionic strength, and isotopic mass on the diffusion coefficients of the dissolved carbonate species. For marine applications, it is also important whether or not there is a significant difference in the diffusion of the carbonate species in dilute solutions vs. seawater. While observations seem to suggest a slightly reduced HCO_3^- mobility in seawater (Fig. 9), the data is too sparse to draw firm conclusions (Kigoshi and Hashitani, 1963; Poisson and Papaud, 1983).

Using molecular dynamics simulations, Bruneval et al. (2007) recently calculated a value of $D_{CO_3^{2-}} \simeq 0.6 \times 10^{-9}$ m^2 s^{-1} at 300 K, which is probably too low (see Fig. 10). The present simulations give $D_{CO_3^{2-}} \simeq 0.8 \times 10^{-9}$ m^2 s^{-1} at 298 K. Also based on MD, Kerisit and Liu (2010) calculated a ratio of $D_{CO_3^{2-}}/D_{H_2O} = 0.353$ at 298.15 K. Using $D_{H_2O} = 2.3 \times 10^{-9}$ m^2 s^{-1}, yields $D_{CO_3^{2-}} = 0.81 \times 10^{-9}$ m^2 s^{-1}, close to the result of the present study.

The results of the MD simulations indicate a small isotope fractionation associated with the diffusion of CO_2, consistent with the reported values for carbon isotope fractionation during $^{12}CO_2/^{13}CO_2$ diffusion of 0.7‰ (25 °C) and 0.87‰ (O'Leary, 1984; Jähne et al., 1987). However, the statistical uncertainties of the simulations prevent precise calculation of the isotope fractionation during diffusion for CO_2, as well as for the ionic carbonate species. The simulations do not suggest a significant isotope fractionation associated with the diffusion of HCO_3^- and CO_3^{2-} at 25 °C. Yet, a small isotope effect cannot be ruled out. For the divalent carbonate anion, a very small (or no) kinetic isotope effect during diffusion is consistent with its stronger solute–solvent interaction, relative to monovalent ions. Experimental and theoretical results also indicate very small (or no) kinetic isotope effects during diffusion of the divalent cations Ca^{2+} and Mg^{2+} (Richter et al., 2006; Bourg et al., 2010).

8. ERRORS AND UNCERTAINTIES OF THE SIMULATIONS

Different classes of errors affect the calculations of diffusion coefficients based on molecular dynamics simulations. First, errors arise due to general limitations of the theoretical method to describe the real physical system. These include simplification and truncations made to derive molecular interaction terms, the limited size of the simulation cell, uncertainties in input values such as Lennard–Jones parameters, etc. Some of those errors have been discussed above (Section 3). On the other hand, errors of statistical nature arise due to the limited time span and/or ensemble size of the simulations, which affect the statistical reliability of the results.

For instance, simulated thermodynamic quantities such as temperature fluctuate significantly around the mean over time. The finite integration time and the correlation of simulation output affect the standard error of the mean of such quantities because the states of consecutive simulation steps, for example, are generally not statistically independent. Because of finite integration times, the limited ensemble size becomes an issue, particularly in the present case where the path of a single dissolved molecule or ion is followed over time. This introduces uncertainties in the calculation of diffusion coefficients because diffusion is a statistical process, which requires averaging over long time intervals and/or large ensembles. Such errors are less problematic for the calculated properties of water, for instance, because the ensemble size is typically much larger (e.g. 215 molecules per cell).

In the following, statistical errors and uncertainties of the simulations will be discussed for temperature and diffusion coefficients based on mean square displacement and velocity autocorrelation function. It is important that these errors are valid within the statistical framework of the molecular dynamics simulations. Their examination is critical for testing whether the results are meaningful in terms of their statistical significance. However, because of the additional limitations mentioned above, the results of the statistical error analyses alone do not imply that the theoretical results have to agree with the true values of the real system within the statistical error bounds obtained.

8.1. Temperature

The typical temperature fluctuation during the simulations was about ± 9 K (Fig. 12). This is the standard deviation of the time series, σ_t, which needs to be explicitly stated in the program output because the printed output is usually averaged over a significant number of time steps. Here, averages were printed every 1000 steps at a time step of 0.001 ps over a total time interval of 500 ps, giving $n_t = 500$ temperature values total. If all states of the series would be uncorrelated (statistically independent), the standard error of the mean would be $S_t = \sigma_t / \sqrt{n_t} = 9 \, \text{K} / \sqrt{500} = 0.4$ K. However, consecutive steps of MD simulations are generally correlated (e.g. Allen and Tildesley, 1987). Following the analysis of Fincham et al. (1986), it turned out that only about half the values are statistically
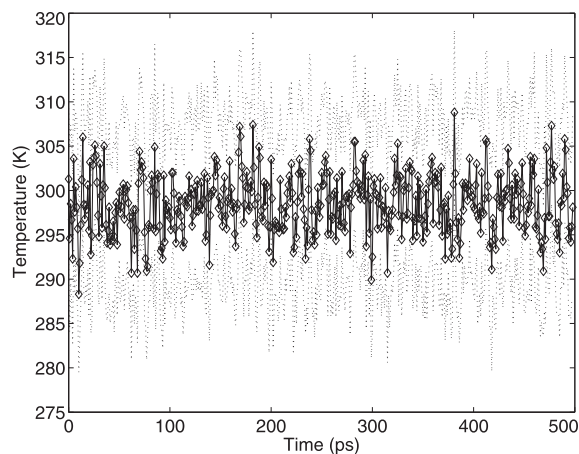

Fig. 12. Typical temperature fluctuations (example: CO_3^{2-} at 298 K) during 500 ps simulation averaged and plotted every 1000 steps at a time step of 0.001 ps (solid line, diamonds) and standard deviation (dotted lines, see text).

independent, i.e. a statistical inefficiency of $\xi \simeq 2$. This corresponds to a correlation time of roughly $500 \, \text{ps}/(500/2) = 2$ ps. Hence $S_t = 9 \, \text{K} / \sqrt{500/2} = 0.57$ K. This is the standard error of the mean temperature for the time series of one simulation over 500 ps (see Table 3).

A total of 16 independent simulations were performed to obtain the ensemble diffusion coefficient of each compound (see Section 3). For instance, for CO_3^{2-} at 298 K, the ensemble mean, standard deviation, and standard error of the mean temperature are $\bar{T}_e = 298.4$ K, $\sigma_e = 0.90$ K, and $S_e = 0.90 \, \text{K} / \sqrt{16} = 0.23$ K (Table 3).

8.2. Mean square displacement

As mentioned above, the diffusion coefficient can be calculated from a fit to the linear part of the mean square displacement (MSD):

$$6 \, D \, t = \langle |\mathbf{r}(t) - \mathbf{r}(0)|^2 \rangle = \text{MSD}(t) \qquad (13)$$

(see Fig. 2a). Taking the time derivative yields:

$$D = \frac{1}{6} \frac{\text{d}}{\text{d}t} \text{MSD}(t) = \text{const.} \qquad (14)$$

Thus for time intervals over which the MSD increases linearly, the right-hand side is constant, except for fluctuations

Table 3
Estimated statistical errors of MD simulations for CO_3^{2-} at 298 K.[a]

Variable	Mean$_e$	σ_e	S_e	(n_e)	CI$_e$	σ_t	S_t	(n_t, ξ)
T(K)	298.4	0.90	0.23	(16)	± 0.45	9.0	0.57	(500, 2)
D_{MSD}[b]	0.52	0.08	0.02	(16)	± 0.04	0.06	0.03	(1700, 350)
D_{VAF}[b]	0.53	0.10	0.03	(16)	± 0.05	0.11[c]	–	–

[a] σ_i = standard deviation, S_i = standard error of the mean, n_i = # ensemble runs or # time series entries, ξ = statistical inefficiency. Subscripts e and t refer to ensemble and time series. CI$_e$ = 95% confidence interval of ensemble runs ($\pm 2 \, \sigma_e / \sqrt{n_e}$), see text.
[b] All values before system-size correction. Unit: 10^{-9} m^2 s^{-1}.
[c] Method to estimate σ_t for D_{VAF} differed from that for T and D_{MSD}, see text.

around the mean. Hence in order to estimate errors in D, a time series analysis analogous to that of temperature may be applied (Fig. 2b). Note, however, that the non-linear part of MSD for $t \to 0$ has to be excluded from the analysis (Allen and Tildesley, 1987). In addition, for large t, the MSD curves show non-linear behavior and larger variability (inlet Fig. 2a). In most cases, this had little effect on the final ensemble mean but increased the range of computed MSD values. Thus the relevant time interval for error analysis was chosen roughly between 1 ps and 10 ps.

Fig. 2b shows $1/6 \times \mathrm{d(MSD)}/\mathrm{d}t$ for three arbitrary runs from the set of 16 for CO_3^{2-} at 298 K. For example, the solid line yields a time series mean and standard deviation of $0.52 \pm 0.06 \times 10^{-9}$ m^2 s^{-1} ($n_t = 1700$). Ignoring correlations, the standard error of the mean would be 0.06×10^{-9} m^2 s$^{-1}/\sqrt{1700} = 0.001 \times 10^{-9}$ m^2 s^{-1}. However, on average only about 5 of the values are statistically independent, i.e. a statistical inefficiency of $\xi \simeq 350$. Hence $S_t = 0.06 \times 10^{-9}$ m^2 s$^{-1}/\sqrt{1700/350} = 0.03 \times 10^{-9}$ m^2 s^{-1}. Note that this yields a correlation time of about 10 ps/5 = 2 ps, consistent with the correlation time obtained for the temperature analysis. The mean diffusion coefficient of the ensemble based on MSD calculations of all 16 runs before system-size correction is 0.52×10^{-9} m^2 s^{-1}, with a standard deviation and standard error of the mean of $\sigma_e = 0.08 \times 10^{-9}$ m^2 s^{-1} and $S_e = 0.02 \times 10^{-9}$ m^2 s^{-1} (Table 3).

8.3. Velocity autocorrelation function

The diffusion coefficient can also be calculated from the velocity autocorrelation function (VAF):

$$D = \frac{1}{3} \int_0^{t_u} \langle |\boldsymbol{v}(t) \cdot \boldsymbol{v}(0)| \rangle \, dt = \frac{1}{3} \int_0^{t_u} \mathrm{VAF}(t) \, dt \qquad (15)$$

where the average runs over particles and time:

$$\mathrm{VAF}(t) = \frac{1}{NN_t} \sum_{i=1}^{N} \sum_{t_0} \boldsymbol{v}_i(t_0 + t) \cdot \boldsymbol{v}_i(t_0). \qquad (16)$$

For large t, the normalized standard deviation of a time correlation function may be estimated according to Zwanzig and Ailawadi (1969), which reads for VAF(t):

$$\sigma_{\mathrm{nVAF}} = \left(\frac{2\tau}{t_r N} \right)^{1/2} \qquad (17)$$

where t_r is the total run time, N is the number of particles, and τ is the mean relaxation time (see below). Note that σ_{nVAF} is normalized to the value of the time correlation function at $t = 0$ (e.g. VAF(0)). Note also that for large t, σ_{nVAF} is independent of time, which means that even after decay of the time correlation function (fluctuating around zero, see Fig. 3), the error remains constant. Zwanzig and Ailawadi (1969) defined the mean relaxation time as:

$$\tau = 2 \int_0^{t_u} dt' \frac{[\mathrm{VAF}(t')]^2}{[\mathrm{VAF}(0)]^2}. \qquad (18)$$

For an exponential decay, τ is equal to the e-folding time and thus shorter than the correlation time discussed above. For instance, for CO_3^{2-} at 298 K the relaxation time τ is about 0.05 ps (Fig. 3), while the correlation time is $\sim$2 ps. Hence for $N = 1$ and 16, the normalized standard deviation of the velocity autocorrelation function, $\sigma_{\mathrm{nVAF}} = [2 \times 0.05 \text{ ps}/(250 \text{ ps} \times N)]^{1/2}$, is about 2% and 0.5% of the initial value VAF(0), respectively.

Note that we only considered the velocity autocorrelation function so far, not the diffusion coefficient. The standard deviation of the diffusion coefficient, calculated by integrating VAF(t) over time (Eq. (15)), may be estimated as follows. For $t < \tau$, the error in VAF(t) is small (Zwanzig and Ailawadi, 1969) and we may focus on the interval where the error estimate (Eq. (17)) is valid, i.e. $\tau < t < t_u$, where t_u is the upper integration limit in Eq. (15). Over this interval, VAF(t) is nearly constant and close to zero, except for fluctuations with constant standard deviation σ_{nVAF}. Hence $\sigma_{D_{\mathrm{VAF}}}$ may be estimated as (see Appendix A):

$$\sigma_{D_{\mathrm{VAF}}} = \frac{1}{3} \frac{t^*}{\sqrt{M}} \sigma_{\mathrm{VAF}} = \frac{1}{3} \frac{t^*}{\sqrt{M}} \mathrm{VAF}(0) \left(\frac{2\tau}{t_r} \right)^{1/2} \qquad (19)$$

where $t^* = t_u - \tau$, M is the number of VAF values over the interval t^*, and σ_{VAF} is the standard deviation of the velocity autocorrelation function for a single run corresponding to Eq. (17). Eq. (19) indicates that the uncertainty in D_{VAF} grows with the upper integration limit t_u for a given M. Thus, in practice the value picked for t_u may be only a few ps (e.g Bourg and Sposito, 2007). Here, D_{VAF} was calculated using the average integrated value between 2 and 4 ps. The VAF was printed every five steps at a time step of 0.001 ps, which, over 4 ps gives $M = 4 \text{ ps}/0.005 \text{ ps} = 800$. Finally, the standard deviation of the calculated diffusion coefficient for a single run for e.g. CO_3^{2-} at 298 K may

Table 4
Results of MD-simulations[a] at $N = 216$ (D^{216}), values at infinite system-size (D^∞), and final values (D, see text).

T (K)	η_{MD} [d]	η_{exp} [d]	H$_2$O[b]			CO$_2$[c]				HCO$_3^-$				CO$_3^{2-}$			
			D^{216}	D^∞	D^{exp}	D^{216}	D^∞	r^∞	D	D^{216}	D^∞	r^∞	D	D^{216}	D^∞	r^∞	D
273	12.5	18.0	1.30	1.55	1.09	1.20	1.45	0.93	1.02	0.48	0.72	0.47	0.51	0.29	0.53	0.34	0.37
298	6.9	8.9	2.37	2.85	2.29	2.03	2.51	0.88	2.02	0.97	1.45	0.51	1.17	0.53	1.01	0.35	0.81
323	4.5	5.5	3.74	4.53	3.94	3.29	4.09	0.90	3.56	1.46	2.26	0.50	1.97	0.82	1.61	0.36	1.40
348	3.9	3.8	5.42	6.40	6.06	4.65	5.63	0.88	5.33	2.16	3.15	0.49	2.98	1.26	2.24	0.35	2.12
373	2.6	2.8	7.48	9.05	8.65	6.21	7.78	0.86	7.44	3.13	4.70	0.52	4.50	1.68	3.25	0.36	3.10

[a] Only values based on VAF are listed.
[b] D's in units of 10^{-9} m^2 s^{-1}.
[c] $r^\infty = D_i^\infty / D_{\mathrm{H_2O}}^\infty$.
[d] Shear viscosity in units of 10^{-4} kg m^{-1} s^{-1}.

be estimated using $t_u = 4$ ps, $\tau = 0.05$ ps, $VAF(0) = 12$ $Å^2 ps^{-2}$, and $\sigma_{nVAF} = 2\%$, which gives $\sigma_{D_{VAF}} = 0.11 \times 10^{-9}$ m^2 s^{-1}.

The mean diffusion coefficient of the ensemble based on VAF calculations of all 16 runs is $0.53 \times 10^{-9} m^2$ s^{-1}, with a standard deviation and standard error of the mean of $\sigma_e = 0.10 \times 10^{-9}$ m^2 s^{-1} and $S_e = 0.03 \times 10^{-9}$ m^2 s^{-1} (Table 3).

8.4. Errors: summary

The analysis of statistical errors above shows that the ensemble standard errors of the mean for D_{MSD} and D_{VAF} are less than $\sim 6\%$ of the respective mean values (Table 3). The corresponding ensemble standard deviations, which provide a measure of the fluctuations around the mean, are less than $\sim 20\%$. The confidence intervals for the calculated diffusion coefficients indicated in the figures were determined based on the ensemble statistics at 95% confidence level ($\pm 2\sigma_e / \sqrt{n_e}$) and scaled based on Eqs. (7) and (8). Given the total time interval of integration and the ensemble size, these uncertainties appear acceptable within the statistical framework of the MD simulations. However, as mentioned above, due to systematic errors, this does not imply that the MD results have to agree with the true values of the diffusion coefficients within the statistical error bounds obtained.

9. CONCLUSIONS

I have used molecular dynamics simulations to study the diffusion of dissolved CO_2, HCO_3^-, and CO_3^{2-} in water. Equations have been provided to calculate the diffusion coefficients of the dissolved carbonate species over the temperature range from 0° to 100 °C. Overall, the MD-calculated results are in good agreement with the sparse observations, given uncertainties in force fields, etc. Furthermore, the results indicate a mass-dependence of CO_2 diffusion that is consistent with the observed $^{12}CO_2/^{13}CO_2$ diffusion ratio at 25 °C (O'Leary, 1984; Jähne et al., 1987). The isotope fractionation associated with the diffusion of naturally occurring isotopologues of HCO_3^- and CO_3^{2-} at 25 °C is probably insignificant.

The theoretical results of the present study are relevant to various research areas dealing with the molecular diffusion of dissolved CO_2, HCO_3^-, and CO_3^{2-}. This includes, for instance, sediment diagenesis, mineral precipitation and dissolution, fossil fuel carbon sequestration, industrial engineering, carbon uptake and calcification in phytoplankton and zooplankton, studies of duodenal ulceration, O_2/CO_2 exchange in red blood cells, and metabolic models of cornea-contact-lens systems (e.g. Berner, 1980; Uchida et al., 1983; Livingston et al., 1995; Wolf-Gladrow and Riebesell, 1997; Cadours and Bouallou, 1998; Zeebe, 2007b; Kaufmann and Dreybrodt, 2007; Berne et al., 2009; Chhabra et al., 2009). Until present, very few experimental data exist on the diffusion coefficients of the ionic carbonate species in water. To the best of my knowledge, no experimental data on $D_{HCO_3^-}$ and $D_{CO_3^{2-}}$ has been obtained for temperatures above 30 °C. The present study

provides values for $D_{HCO_3^-}$ and $D_{CO_3^{2-}}$ up to 100 °C. The values of 0.92 and 0.96×10^{-9} m^2 s^{-1} for $D_{CO_3^{2-}}$ at 25 °C (Robinson and Stokes, 1959; Li and Gregory, 1974) that have been widely used in the literature and cited in textbooks (e.g. Boudreau, 1997; Reddi and Inyang, 2000; Hudak, 2005) are probably too high by 15–20%. This can lead, for instance, to overestimates of the carbonate dissolution flux from sediments, which is proportional to $D_{CO_3^{2-}}$ (e.g. Keir, 1982; Boudreau and Guinasso, 1982; Zeebe, 2007b).

It also appears that no information was hitherto available on the mass-dependence of the diffusion coefficients of the ionic carbonate species in water. In the past, it has generally been assumed that no fractionation is associated with $H^{12}CO_3^-/H^{13}CO_3^-$ and $^{12}CO_3^{2-}/^{13}CO_3^{2-}$ diffusion, respectively (e.g. McCorkle et al., 1985; Gehlen et al., 1999; Zeebe, 2007a). The present results justify this assumption. Likewise, no significant effect on the diffusion coefficients of HCO_3^- and CO_3^{2-} appears to be associated with the substitution of naturally occurring stable oxygen isotopes (or the various combinations of $^{12}C, ^{13}C, ^{16}O, ^{17}O$, and ^{18}O). This has implications, for instance, for understanding vital effects in carbonates and clumped isotope studies (e.g. Thiagarajan et al., 2009). Beyond the theoretical results obtained here, a comprehensive experimental study on the diffusion of the ionic carbonate species appears desirable to examine various parameters such as temperature, solute concentrations, ionic strength, and isotopic mass.

APPENDIX A. QUADRATURE ERROR PROPAGATION

Calculation of the diffusion coefficient from the velocity autocorrelation function (VAF) requires integration of the VAF over a certain time interval (Section 8.3). This is usually accomplished via a quadrature approximation of the integral. In the following, an estimate is provided for the standard deviation of the integrated result, given the standard deviation of the integrand. Consider a function $f(t), 0 \leqslant t \leqslant t^*$, represented at discrete times t_i by $f'(t_i) = y_i$ with standard deviations σ_{y_i}, where $t_i = (i - 1) \times \Delta t$ and $i = 1, \ldots, M + 1$. For simplicity, the integral may be approximated by:

$$\int_0^{t^*} f'(t) \, dt \simeq F(y_1, y_2, \ldots, y_M) = \sum_{i=1}^{M} h \times y_i \qquad (A1)$$

where $h = \Delta t$ and the total integration interval is $t^* = M h$. Note that the integral approximation is reasonable only for large M (the trapezoidal rule or Simpson's rule may be used

for small M). Given uncorrelated standard deviations σ_{y_i}, the variance, σ_F^2, is:

$$\sigma_F^2 = \left(\frac{\partial F}{\partial y_1}\right)^2 \sigma_{y_1}^2 + \left(\frac{\partial F}{\partial y_2}\right)^2 \sigma_{y_2}^2 + \cdots + \left(\frac{\partial F}{\partial y_M}\right)^2 \sigma_{y_M}^2 \quad (A2)$$

$$= \sum_{i=1}^{M} \left(\frac{\partial F}{\partial y_i}\right)^2 \sigma_{y_i}^2 = \sum_{i=1}^{M} h^2 \sigma_{y_i}^2 \quad (A3)$$

If the standard deviations σ_{y_i} are constant and equal to σ_y (as is the case for the VAF at $t > \tau$), then $\sigma_F^2 = M \times h^2 \, \sigma_y^2$ or $\sigma_F = \sqrt{M} \times h \, \sigma_y$. Using $\sqrt{M} = M/\sqrt{M}$ and $M \, h = t^*$, we have

$$\sigma_F = \frac{t^*}{\sqrt{M}} \, \sigma_y. \quad (A4)$$

REFERENCES

Allen M. P. and Tildesley D. J. (1987) *Computer Simulation of Liquids*. Springer, Berlin, p. 385.

Berendsen H. J. C., Grigera J. R. and Straatsma T. P. (1987) The missing term in effective pair potentials. *J. Phys. Chem.* **91**(24), 6269–6271. doi:10.1021/j100308a038.

Berne P., Bachaud P. and Fleury M. (2009) Diffusion properties of carbonated caprocks from the Paris Basin. *Oil Gas Sci. Technol. Rev. IFP.* doi:10.2516/ogst/2009072.

Berner R. A. (1980) *Early Diagenesis: A Theoretical Approach*. Princeton University Press, Princeton, p. 241.

Boudreau B. P. (1997) *Diagenetic Models and their Implementation*. Springer, New York, p. 414.

Boudreau B. P. and Guinasso N. L. (1982) The influence of a diffusive sublayer on accretion, dissolution and diagenesis at the sea floor. In *The Dynamic Environment of the Ocean Floor* (eds. K. A. Fanning and F. T. Manheim). Lexington Books, pp. 115–145.

Bourg I. C., Richter F. M., Christensen J. N. and Sposito G. (2010) Isotopic mass dependence of metal cation diffusion coefficients in liquid water. *Geochim. Cosmochim. Acta* **74**, 2249–2256.

Bourg I. C. and Sposito G. (2007) Molecular dynamics simulations of kinetic isotope fractionation during the diffusion of ionic species in liquid water. *Geochim. Cosmochim. Acta* **71**, 5583–5589.

Bourg I. C. and Sposito G. (2008) Isotopic fractionation of noble gases by diffusion in liquid water: molecular dynamics simulations and hydrologic applications. *Geochim. Cosmochim. Acta* **72**, 2237–2247.

Bruneval F., Donadio D. and Parrinello M. (2007) Molecular dynamics study of the solvation of calcium carbonate in water. *J. Phys. Chem. B* **111**, 12219–12227.

Cadours R. and Bouallou C. (1998) Rigorous simulation of gas absorption into aqueous solutions. *Ind. Eng. Chem. Res.* **37**(3), 1063–1070.

Chapman S. and Cowling T. G. (1970) *The Mathematical Theory of Non-uniform Gases*, third ed. University Press, Cambridge.

Chhabra M., Prausnitz J. M. and Radke C. J. (2009) Modeling corneal metabolism and oxygen transport during contact lens wear. *Optom. Vis. Sci.* **86**(5), 454–466.

Cussler E. L. (1984) *Diffusion. Mass Transfer in Fluid Systems*. Cambridge University Press, New York, p. 525.

Davidson J. F. and Cullen E. J. (1957) The determination of diffusion coefficients for sparingly soluble gases in liquids. *Chem. Eng. Res. Design* **35a**, 51–60.

Duffy D. M., Travaille A. M., van Kempen H. and Harding J. H. (2005) Effect of bicarbonate ions on the crystallisation of calcite on self-assembled monolayers. *J. Phys. Chem. B* **109**(14), 5713–5718.

Dünweg B. and Kremer K. (1991) Microscopic verification of dynamic scaling in dilute polymer solutions: a molecular-dynamics simulation. *Phys. Rev. Lett.* **66**, 2996–2999.

Dünweg B. and Kremer K. (1993) Molecular dynamics simulation of a polymer chain in solution. *J. Chem. Phys.* **99**, 6983–6997.

Einstein A. (1905) Über die von der molekularkinetischen Theorie der Wärme geforderte Bewegung von in ruhenden Flüssigkeiten suspendierten Teilchen. *Ann. Phys.* **322**, 549–560.

Fincham D., Quirke N. and Tildesley D. J. (1986) Computer simulation of molecular liquid mixtures, Part I: A diatomic Lennard–Jones model mixture for CO_2/C_2H_6. *J. Chem. Phys.* **84**(8), 4535–4546.

Garand E., Wende T., Goebbert D. J., Bergmann R., Meijer G., Neumark D. M. and Asmis K. R. (2010) Infrared spectroscopy of hydrated bicarbonate anion clusters: $HCO_3^-(H_2O)_{1-10}$. *J. Am. Chem. Soc.* **132**(2), 849–856.

Gehlen M., Mucci A. and Boudreau B. P. (1999) Modelling the distribution of stable carbon isotopes in porewaters of marine sediments. *Geochim. Cosmochim. Acta* **63**(18), 2763–2773.

Gordon M. S. and Schmidt M. W. (2005) Advances in electronic structure theory: GAMESS a decade later. In *Theory and Applications of Computational Chemistry: The First Forty Years* (eds. G. Frenking, K. S. Kim and G. E. Scuseria). Elsevier, Amsterdam, pp. 1167–1189.

Hansen J.-P. and McDonald I. R. (2006) *Theory of Simple Liquids*. Elsevier, Amsterdam, p. 416.

Hashitani T. and Kigoshi K. (1965) Measurements of the self-diffusion coefficients of carbon dioxide, hydrogen carbonate ions and carbonate ions in aqueous solution. *Bull. Chem. Soc. Jpn.* **38**(8), 1395–1396.

Himmelblau D. M. (1964) Diffusion of dissolved gases in liquids. *Chem. Rev.* **64**(5), 527–550.

Holz M., Heil S. R. and Sacco A. (2000) Temperature-dependent self-diffusion coefficients of water and six selected molecular liquids for calibration in accurate ^1H NMR PFG measurements. *Phys. Chem. Chem. Phys.* **2**, 4740–4742.

Huber M. L., Perkins R. A., Laesecke A., Sengers J. V., Friend D. G., Assael M. J., Metaxa I. N., Vogel E., Mares R. and Miyagawa K. (2009) New international formulation for the viscosity of H_2O. *J. Phys. Chem. Ref. Data* **38**(2), 101–125.

Hudak P. F. (2005) *Principles of Hydrogeology*, third. ed. CRC Press, Boca Raton, FL, p. 248.

Humphrey W., Dalke A. and Schulten K. (1996) VMD – visual molecular dynamics. *J. Mol. Graph.* **14**, 33–38, <http://www.ks.uiuc.edu/Research/vmd>.

Hyun J.-K., Johnston K. P. and Rossky P. J. (2001) Structural and dynamical origins of ionic mobilities in supercritical water. *J. Phys. Chem. B* **105**, 9302–9307.

in het Panhuis M., Patterson C. H. and Lynden-Bell R. M. (1998) A molecular dynamics study of carbon dioxide in water: diffusion, structure and thermodynamics. *Mol. Phys.* **94**, 963–972.

Jähne B., Heinz G. and Dietrich W. (1987) Measurement of the diffusion coefficients of sparingly soluble gases in water. *J. Geophys. Res.*(10), 10767–10776.

Kalinichev A. G. (1993) Molecular dynamics and self-diffusion in supercritical water. *Ber. Bunsenges. Phys. Chem.* **97**(7), 872–876.

Kalinichev A. G., Wang J. and Kirkpatrick R. J. (2001) Structure of carbonate and bicarbonate aqueous solutions: molecular simulation of ionic hydration and ion pairing. *In 11th Goldschmidt Conference, Abstract No. 3293.*

Kaufmann G. and Dreybrodt W. (2007) Calcite dissolution kinetics in the system $CaCO_3$–H_2O–CO_2 at high undersaturation. *Geochim. Cosmochim. Acta* **71**, 1398–1410.

Keir R. (1982) Dissolution of calcite in the deep sea: theoretical predictions for the case of uniform size particles settling into a well-mixed sediment. *Am. J. Sci.* **282**, 193–236.

Kerisit S. and Liu C. (2010) Molecular simulation of the diffusion of uranyl carbonate species in aqueous solution. *Geochim. Cosmochim. Acta* **74**, 4937–4952.

Kestin J., Knierim K., Mason E. A., Najafi B., Ro S. T. and Waldman M. (1984) Equilibrium and transport properties of the noble gases and their mixtures at low density. *J. Phys. Chem. Ref. Data* **13**, 229–303.

Kigoshi K. and Hashitani T. (1963) The self-diffusion coefficients of carbon dioxide, hydrogen carbonate ions and carbonate ions in aqueous solutions. *Bull. Chem. Soc. Jpn.* **36**(10), pp. 1372–1372.

Koneshan S., Rasaiah J. C., Lynden-Bell R. M. and Lee S. H. (2001) Solvent structure, dynamics, and ion mobility in aqueous solutions at 25 °C. *J. Phys. Chem.* **102**, 4193–4204.

Kumar P. P., Kalinichev A. G. and Kirkpatrick R. J. (2009) Hydrogen-bonding structure and dynamics of aqueous carbonate species from Car to Parrinello molecular dynamics simulations. *J. Phys. Chem. B* **113**, 794–802.

Landolt-Börnstein (1960) *Zahlenwerte und Funktionen aus Physik, Chemie, Astronomie, Geophysik und Technik*. Springer, Berlin, pp. 257–275 (II. Band, 7. Teil).

Leote de Carvalho R. J. F. and Skipper N. T. (2001) Atomistic computer simulation of the clay–fluid interface in colloidal laponite. *J. Chem. Phys.* **114**, 3727–3733.

Leung K., Nielsen I. M. B. and Kurtz I. (2007) Ab initio molecular dynamics study of carbon dioxide and bicarbonate hydration and the nucleophilic attack of hydroxide on CO_2. *J. Phys. Chem. B* **111**, 4453–4459.

Li T., Kheifets S., Medellin D. and Raizen M. G. (2010) Measurement of the instantaneous velocity of a Brownian particle. *Science* **328**, 1673–1675.

Li Y.-H. and Gregory S. (1974) Diffusion of ions in sea water and in deep-sea sediments. *Geochim. Cosmochim. Acta* **38**, 703–714.

Livingston E. H., Miller J. and Engel E. (1995) Bicarbonate diffusion through mucus. *Am. J. Physiol. Gastrointest. Liver. Physiol.* **269**, G453–G457.

McCorkle D. C., Emerson S. R. and Quay P. D. (1985) Stable carbon isotopes in marine porewaters. *Earth Planet. Sci. Lett.* **74**, 13–26.

Monk C. B. (1949) The conductivity of sodium carbonate solutions at 25 °C. *J. Chem. Soc.*, 429–431.

O'Leary M. H. (1984) Measurement of the isotope fractionation associated with diffusion of carbon dioxide in aqueous solution. *J. Phys. Chem.* **88**, 823–825.

Poisson A. and Papaud A. (1983) Diffusion coefficients of major ions in seawater. *Mar. Chem.* **13**(4), 265–280.

Rahman A. (1964) Correlations in the motion of atoms in liquid argon. *Phys. Rev.* **136**(2A), 405–411.

Raiteri P., Gale J. D., Quigley D. and Rodger P. M. (2010) Derivation of an accurate force-field for simulating the growth of calcium carbonate from aqueous solution: a new model for the calcite-water interface. *J. Phys. Chem. C* **114**(13), 5997–6010.

Reddi L. N. and Inyang H. I. (2000) *Geoenvironmental Engineering: Principles and Applications*. Marcel Dekker Publishing Co., New York, p. 494.

Refson K. (2000) Moldy: a portable molecular dynamics simulation program for serial and parallel computers. *Comput. Phys. Commun.* **126**, 310–329.

Richter F. M., Mendybaev R. A., Christensen J. N., Hutcheon I. D., Williams R. W., Sturchio N. C. and Beloso A. D. (2006) Kinetic isotopic fractionation during diffusion of ionic species in water. *Geochim. Cosmochim. Acta* **70**, 277–289.

Robinson R. A. and Stokes R. H. (1959) *Electrolyte Solutions*, second ed. Butterworth's, London, p. 559.

Rustad J. R., Nelmes S. L., Jackson V. E. and Dixon D. A. (2008) Quantum-chemical calculations of carbon-isotope fractionation in $CO_2(g)$, aqueous carbonate species, and carbonate minerals. *J. Phys. Chem. A* **112**, 542–555.

Shedlovsky T. and MacInnes D. A. (1935) The first ionization constant of carbonic acid, 0 to 38 °C, from conductance measurements. *J. Am. Chem. Soc.* **57**, 1705–1710.

Speedy R. J. and Angell C. A. (1976) Isothermal compressibility of supercooled water and evidence for a thermodynamic singularity at −45 °C. *J. Chem. Phys.* **65**, 851–858.

Tamimi A., Rinker E. B. and Sandall O. C. (1994) Diffusion coefficients for hydrogen sulfide, carbon dioxide, and nitrous oxide in water over the temperature range 293–368 K. *J. Chem. Eng. Data* **39**, 330–332.

Tegeler C., Span R. and Wagner W. (1999) A new equation of state for Argon covering the fluid region for temperatures from the melting line to 700 K at pressures up to 1000 MPa. *J. Phys. Chem. Ref. Data* **28**, 779–850.

Thiagarajan N., Guo W., Adkins J. and Eiler J. (2009) Clumped isotope calibration of modern deep sea corals and implications for vital effects. *Geochim. Cosmochim. Acta Suppl.* **73**, 1324.

Thomas W. J. and Adams M. J. (1965) Measurement of the diffusion coefficients of carbon dioxide and nitrous oxide in water and aqueous solutions of glycerol. *Trans. Faraday Soc.* **61**, 668–673.

Uchida K., Mochizuki M. and Niizeki K. (1983) Diffusion coefficients of CO_2 molecule and bicarbonate ion in hemoglobin solution measured by fluorescence technique. *Jpn. J. Physiol.* **33**, 619–634.

Wang J. and Becker U. (2009) Structure and carbonate orientation of vaterite ($CaCO_3$). *Am. Mineral.* **94**, 380–386.

Winn E. B. (1950) The temperature dependence of the self-diffusion coefficients of argon, neon, nitrogen, oxygen, carbon dioxide, and methane. *Phys. Rev.* **80**(6), 1024–1027.

Wolf-Gladrow D. A. and Riebesell U. (1997) Diffusion and reactions in the vicinity of plankton: a refined model for inorganic carbon transport. *Mar. Chem.* **59**, 17–34.

Yeh I.-C. and Hummer G. (2004) System-size dependence of diffusion coefficients and viscosities from molecular dynamics simulations with periodic boundary conditions. *J. Phys. Chem. B* **108**, 15873–15879.

Zeebe R. E. (1999) An explanation of the effect of seawater carbonate concentration on foraminiferal oxygen isotopes. *Geochim. Cosmochim. Acta* **63**, 2001–2007.

Zeebe R. E. (2007a) An expression for the overall oxygen isotope fractionation between the sum of dissolved inorganic carbon and water. *Geochem. Geophys. Geosyst.* **8**(9), Q09002. doi:10.1029/2007GC001663.

Zeebe R. E. (2007b) Modeling CO_2 chemistry, $\delta^{13}C$, and oxidation of organic carbon and methane in sediment porewater: Implications for paleo-proxies in benthic foraminifera. *Geochim. Cosmochim. Acta* **71**, 3238–3256.

Zeebe R. E. (2009) Hydration in solution is critical for stable oxygen isotope fractionation between carbonate ion and water. *Geochim. Cosmochim. Acta* **73**, 5283–5291.

Zeebe R. E. (2010) A new value for the stable oxygen isotope fractionation between dissolved sulfate ion and water. *Geochim. Cosmochim. Acta* **74**, 818–828.

Zeebe R. E., Jansen H. and Wolf-Gladrow D. A. (1999) On the time required to establish chemical and isotopic equilibrium in the carbon dioxide system in seawater. *Mar. Chem.* **65**, 135–153.

Zeebe R. E. and Wolf-Gladrow D. A. (2001) CO_2 *in Seawater: Equilibrium, Kinetics, Isotopes.* Elsevier Oceanography Series, Amsterdam, p. 346.

Zwanzig R. and Ailawadi N. K. (1969) Statistical error due to finite time averaging in computer experiments. *Phys. Rev.* **182**, 280–283.

Associate editor: William H. Casey